Evidence for a Copper-Binding Superfamily of the Amyloid Precursor Protein[†]

Andreas Simons,[‡] Thomas Ruppert,[‡] Carsten Schmidt,[‡] Andrea Schlicksupp,[‡] Rüdiger Pipkorn,[§] Jennifer Reed,[§] Colin L. Masters,[∥] Anthony R. White,[∥] Roberto Cappai,[∥] Konrad Beyreuther,[‡] Thomas A. Bayer,[⊥] and Gerd Multhaup*,[‡]

ZMBH—Center for Molecular Biology, University of Heidelberg, Im Neuenheimer Feld 282, D-69120 Heidelberg, Germany, German Cancer Research Center, Im Neuenheimer Feld 506, Heidelberg D-69120, Germany, Department of Pathology, The University of Melbourne, Victoria 3010, Australia, The Mental Health Research Institute, Parkville, Victoria 3052, Australia, and University of Bonn Medical Center, Department of Psychiatry, Sigmund-Freud-Strasse 25, D-53105 Bonn, Germany

Received March 25, 2002; Revised Manuscript Received May 3, 2002

ABSTRACT: The amyloid precursor protein (APP) copper-binding domain (CuBD) has been shown to reduce Cu(II) to Cu(I) and to mediate copper-induced oxidation in vitro. However, little is known about copper binding to the homologous domains of APP and APP family paralogs and orthologs (including amyloid precursor-like proteins from *Drosophila melanogaster*, *Xenopus laevis*, and *Caenorhabditis elegans*) and their effects on Cu-induced oxidation and Cu(I) formation. Here, we show that APP homologues with and without conserved histidine residues at positions 147, 149, and 151 all bind Cu(II). Oxidized peptides were the kinetically favored products of the redox reaction of CuBDs promoting the reduction of Cu(II) to Cu(I). These results reveal a molecular phylogeny-based divergence that has taken place between the ancestral *Drosophila* APPL and *C. elegans* APL-1 and the recently evolved APP lineage of CuBDs. Whereas higher species CuBDs have a decreased affinity for Cu(II) and high Cu(II) reducing activities, ancestral CuBDs form very tight binding sites for Cu(II) ions and have low Cu(II) reducing activities. Thus, the APP lineage displays a gain in activity toward promoting Cu(II) reduction and Cu(I) release. The findings suggests that the Cu(II)-binding equilibrium at the phylogenetic stage of *Drosophila* APPL and *C. elegans* APL-1 is shifted from the exchangeable Cu(II) pool to the tightly bound, nonexchangeable pool and that ancestral CuBDs may exert antioxidation activities in vivo. The more recently evolved homologues of human APP appear to take advantage of unique redox properties for yet unknown biological functions.

Several fatal neurodegenerative disorders such as Alzheimer's disease (AD)[1], familial amyothrophic lateral sclerosis (FALS), and prion-related diseases (also known as transmissible spongiform encephalopathies) are associated with the misfolding of a Cu-binding protein that is central to the specific disease (*1*−*9*). An altered copper homeostasis may be involved in the pathogenetic process in these disorders, either due to an aberrant metal binding by the prion protein in human transmissible spongiform encephalopathies (*10*), an altered cellular copper chemistry of ALS mutant Cu/Zn superoxide dismutase (SOD1), or Cu-induced oxidation and Cu(I) formation by the amyloid precursor protein (APP) of Alzheimer's disease (*11*−*13*).

APP strongly binds copper, and this leads to oxidation of residues Cys144 and Cys158 of APP in vitro (*13*). The copper-binding domain of APP is located in the N-terminal cysteine-rich region which is of critical importance for the regulation of homooligomerization of full-length APP that occurs during cellular synthesis (*14*, *15*). Copper binding to APP reduces Aβ production to undetectable levels and stimulates the nonamyloidogenic pathway of APP metabolism (ref *16* and Multhaup, G., Schmidt, C., and Simons, A., to be submitted for publication).

Recently, the neuronal adaptor protein X11α has been described as a molecule that links intracellular Cu homeostasis and intracellular trafficking of APP. X11α mediates the interactions between presenilin-1 and APP (*17*) and regulates SOD1 activity through a direct interaction with the copper chaperone for SOD, termed CCS (*18*). A possible role for APP in modulating copper homeostasis was established by showing that APP$^{0/0}$ mice have elevated copper

[†] This work was supported in part by grants from the DFG (MU901), DFG Grossgeräte Sachbeihilfe to the ZMBH (through K.B. and G.M.), and the Fonds der Chemischen Industrie (through K.B.). C.L.M. and R.C. were supported in part by grants from the National Health and Medical Research Council of Australia.

* Corresponding author. Phone: +49-6221-546849. Fax: +49-6221-545891. E-mail: g.multhaup@zmbh.uni-heidelberg.de.

[‡] University of Heidelberg.

[§] German Cancer Research Center.

[∥] The University of Melbourne and The Mental Health Research Institute.

[⊥] Department of Psychiatry.

[1] Abbreviations: Aβ, amyloid peptide; APP, amyloid precursor protein; xAPP, *Xenopus laevis* amyloid precursor-like protein; APLP1, amyloid precursor-like protein 1; APLP2, amyloid precursor-like protein 2; APL-1, *Caenorhabditis elegans* amyloid precursor-like protein; APPL, *Drosophila melanogaster* amyloid precursor-like protein; BC, bathocuproine disulphonate; CD, circular dichroism; CCS, copper chaperone for superoxide dismutase 1 (SOD1); CuBD, copper-binding domain; DTT, dithiothreitol; FALS, familial amyotrophic lateral sclerosis; HPLC, high-performance liquid chromatography; ICP-MS, inductively coupled plasma mass spectrometry; IDA, iminodiacetic acid; NTA, nitrilotriacetic acid; Q-TOF, quadrupole time-of-flight; ROS, reactive oxygen species; RU, response unit; SOD1, copper/zinc-superoxide dismutase; SPR, surface plasmon resonance; TCEP, tris-(2-carboxyethyl)phosphine.

10.1021/bi0258647 CCC: $22.00
Published on Web 06/28/2002

Table 1: APP_{CuBD}, Homologs thereof, and Two Peptide Variants Harboring Mutations[a]

Peptide	Sequence (137 147 151)	charge-state +5	MW calcd. [Da]	Cu-activity*
APP CuBD	FL**H**QERMDV*C* ET**H**L**H**W**H**TVAKET*C* SEKSTNLH	m/z 770.1638	3845.7800	Toxic
APP CuBD N137	FL**N**QERMDV*C* ET**H**L**H**W**H**TVAKET*C* SEKSTNLH	m/z 765.5612	3822.7666	Toxic
APLP2 CuBD	FF**H**KERMEV*C* EN**H**Q**H**W**H**TVVKEA*C* LTQGMTLY	m/z 787.1721	3930.8215	Toxic
APLP1 CuBD	FL**H**QERMDQ*C* ESSTRR**H**QEAQEA*C* SSQGLILH	m/z 751.7510	3753.7158	Inert
xAPP CuBD	FL**H**QERMDI*C* ET**H**L**H**W**H**TVAKES*C* SEKSMSLH	m/z 770.7607	3848.7644	Toxic
APL-1 CuBD	FS**H**VNSRDQ*C* NDYQ**H**WKDEAGKQ*C* KTKKSKGN	m/z 754.1576	3765.7488	Protective
APPL CuBD	FD**H**I**H**NASR*C* WPFVRWNQTGAAA*C* QERGMQMR	m/z 761.5548	3802.7351	Protective
APP CuBD Y147.K151	FL**H**QERMDV*C* ETYL**H**WKTVAKET*C* SEKSTNLH	n.d.	n.d.	Protective

[a] (*) The terms toxic, protective, and inert indicate the activity of the peptides towards Cu-mediated activities (according to ref *28*).

levels in the cerebral cortex (*19*), whereas Cu levels in transgenic APP mice (an animal model of AD) were found to be slightly reduced (Multhaup, G., Schmidt, C., and Simons, A., to be submitted for publication). In addition, we have observed that APP is prominently present in human bile (Multhaup, G., and Stremmel, W., unpublished observation) and that biliary excretion represents the sole physiological mechanism for copper excretion (*20*).

Although redox-cycling between Cu(II) and Cu(I) is used under physiological conditions by cuproenzymes (e.g., Cu/Zn superoxide dismutase or cytochrome *c* oxidase), this redox property is believed to contribute to the inherent toxicity of this essential element (*21*) and to play a role in the initiation or progression of neurodegenerative diseases including AD. In fact, oxidative stress in AD has been described as the consequence of damaging reactive oxygen species such as hydroxyl radicals (*7*, *22*−*24*), which are generated through Fenton-like chemistry between lower valence metal cations (e.g., Fe(II) and Cu(I)) and hydrogen peroxide (*25*−*27*). In cell culture and cell-free lipid peroxidation assays, Cu-mediated toxicity could be mapped to the proposed copper-binding domain of APLP2 and nonmammalian APP orthologs. APP orthologs with amino acid changes within this domain had altered phenotypes (*28*). Interestingly, the *Caenorhabditis elegans* amyloid precursor-related protein APL-1 strongly protected against Cu toxicity and conferred a protective phenotype (*28*). Most likely, *C. elegans* amyloid precursor-related protein APL-1 had antioxidation activity and could thereby prevent reactive oxygen species (ROS) formation.

We have examined CuBDs which are homologous to the respective APP domain including *C. elegans* amyloid precursor-related protein APL-1 (the common ancestral protein of APP and APLP), *Drosophila melanogaster* APPL, and *Xenopus laevis* APP in Cu binding and reducing activities by utilizing a modified surface plasmon resonance (SPR) assay, Q-TOF mass spectrometry, and ICP mass spectrometry. We observed that (i) APP homologues with and without conserved histidine residues all bind Cu(II), (ii) oxidized peptides are the kinetically favored products of the redox reaction of all CuBDs, and (iii) divergent Cu(II) binding and reducing activities correlate with the phylogenetic position of the CuBD.

EXPERIMENTAL PROCEDURES

Chemical Synthesis, Purification, and Analysis of Synthetic Peptides. For solid-phase synthesis of APP_{CuBD} peptides (Table 1), we employed the Fmoc strategy (*29*, *30*) in a fully automated synthesizer (ABI 433). Peptide chain assembly was performed using in situ activation of amino acid building blocks by 2-(1*H*-benzotriazole-1-yl)-1,1,3,3-tetramethyluronium hexafluorophosphate (HBTU). The purified material was analyzed by HPLC and laser desorption mass spectrometry (Vision 2000, Finnigan MAT, San Jose, CA). Purified peptides were lyophilized and stored at −20 °C until use.

Concentrations of dissolved peptides were determined by amino acid analysis according to the manufacturer's protocol after hydrolysis with 6 N HCl, 0.1% phenol for 24 h at 110 °C (420A Amino Acid Analysis System, Applied Biosystems, Foster City, CA).

HPLC of CuBD Peptides. Reversed-phase HPLC was performed at room temperature on a Hewlett-Packard/Agilent Series 1100 liquid chromatography system equipped with a Pharmacia Biotech μRPC-C2/C18 column. Peptides were injected from freshly prepared stock solutions (100 μL from a solution of 100 μg/mL peptide in 0.1 μM EDTA with or without 30 μM $CuCl_2$) and eluted with a gradient beginning with solvent A (10 mM ammonium acetate, pH 6.5) and an increasing percentage of solvent B (10 mM ammonium acetate/70% acetonitrile, pH 6.5). The separations were carried out at a flow rate of 250 μL/min using a linear gradient within 30 min, followed by reequilibration to buffer A for 5 min, and were monitored at 216 nm.

Real-Time SPR Analysis (BIACORE). Real-time binding experiments were performed on a BIACORE system equipped with the upgrade kit (BIACORE, Uppsala, Sweden). All experiments were performed at 37 °C. Sensor chip NTA (sensor chip NTA, BIACORE), originally designed to bind histidine-tagged molecules for interaction analysis in BIACORE instruments via nickel-saturated NTA, was used to establish a new biosensor assay. Instead of attaching ligands via histidine tags to a nickel charged NTA surface, the methodology elaborated here relies on the binding of synthetic peptides derived from the CuBD sequence of APP to an NTA-chelated copper atom. Peptide concentration and contact time was used to control the amount of peptide bound to NTA−Cu.

Prior to all binding experiments, the sensor chip−NTA surface was conditioned by injecting 20 μL of 50 mM EDTA followed by an EXTRACLEAN command to thoroughly clean the liquid handling system to avoid a carry-over of EDTA into the following injection. To prepare a metal chelating sensor surface, the nitrilotriacetic acid immobilized

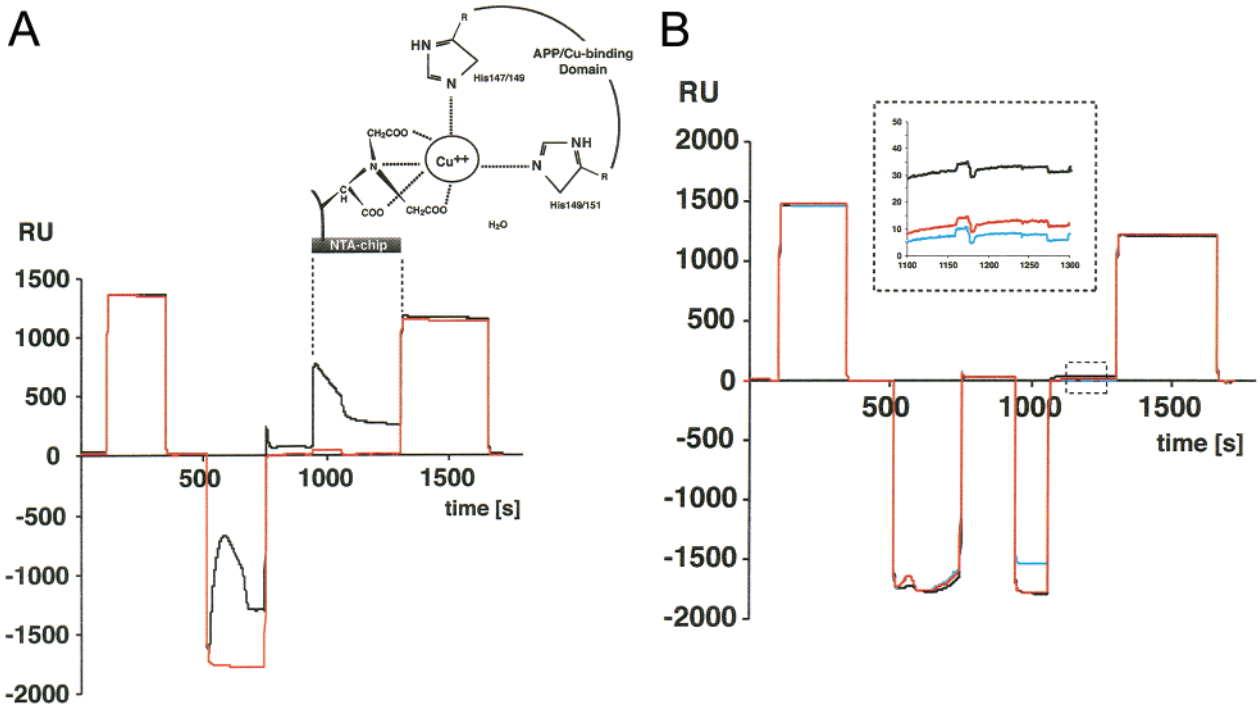

FIGURE 1: (A) Overlay of sensorgrams showing the specific binding of the APP_{CuBD} peptide to copper-charged NTA and the principle of Cu(II) binding to the NTA. Interaction of the APP_{CuBD} with Cu(II)−NTA (black curve) and the absence of interaction (red curve) with metal-free NTA (i.e., not previously loaded with Cu(II)). Soft histidine-imidazole nitrogens surround the copper atom in a manner simulating the Cu/Zn−SOD situation (*47*). The NTA group has four chelating sites that interact with four of the six coordination sites of the metal ion (e.g., Cu(II)). The sensor chip was preconditioned by injecting 20 μL of 50 mM EDTA to remove residual metal ions on the chip surface (120−320 s) followed by a 4-min pulse of the copper solution (causing an increase of the baseline level of ~30 RU) to saturate the NTA with Cu(II) (black curve). Alternatively, 1 μM EDTA was injected without causing a change in the baseline (red curve). Upon injection of APP_{CuBD}, the peptide rapidly binds to Cu(II)−NTA (at ~950 s) before a displacement of Cu(I)−peptide complexes occurs due to a residual reducing activity of APP_{CuBD} (~950 to ~1100 s) followed by a dissociation of the APP_{CuBD} from the Cu(II)−NTA surface (from ~1100 to ~1300 s, shown here under reducing conditions in the presence of TCEP). Note that the rectangular increase of the red curve (~950 to ~1100 s) is due to a nonspecific increase of the refractive index by the dissolved APP_{CuBD}. The NTA sensor chip surface was regenerated by stripping Cu(II) from the surface with 30 μL of 50 mM EDTA (the rectangular increases of red and black curves from ~1300 to ~1650 s). (B) Experimental proof of divalent copper ion binding to NTA, covalently immobilized to a carboxymethylated dextran sensor chip matrix. The regeneration solution was injected to remove metal ions that may have been present in previously used reagents (120−320 s) followed by a 4-min pulse of the copper solution to saturate the NTA with Cu(II) producing an increase of the baseline level of ~30 RU after the injection (at 720 s). During the injection of BC (black curve), the increased baseline remained constant, whereas TCEP (red curve) and vitamin C (blue curve) solutions stripped copper from the surface (inset) and the baseline almost reached the level before the injection of Cu(II). To regenerate the sensor chip NTA, a 5-min pulse of the regeneration solution was injected (1300−650 s). Note that the stripping of copper from the surface only occurs in the presence of a soluble reducing compound or EDTA but not in the presence of BC.

sensor chip was exposed to copper solution (100 μM $CuCl_2$ in Milli-Q water) for 4 min at a flow rate of 5 μL/min. This produced an increase of the baseline level of 30−40 RU (Figure 1B). For nonmetal experiments, the sensor surface was treated as previously described except that EDTA (1 μM) was injected for 4 min. Peptide samples were freshly dissolved to 1 mg/mL in 1 μM EDTA in Milli-Q water to minimize contaminations of metal ions. Peptide stock solutions were diluted to 30 μg/mL in 1 × PBS and either 10 μL (equals 300 ng) was injected onto the NTA−Cu surface or the solutions were adjusted to 2 mM TCEP, 100 μM BC, or 1 mM vitamin C before injection.

The sample recovery feature (BIACORE Upgrade Instrument Handbook, 1995) was used to recover the injected synthetic peptide by diverting the effluent from the integrated flow cartridge to the recovery cup on the connector block of the machine. The RECOVER command was placed immediately after the INJECT command to which it applied. To ensure complete recovery of all of the injected peptide, a 20 μL volume (10 μL more than the volume of sample injected) was specified in the command table for recovery. The NTA sensor chip was regenerated by stripping Cu(II) from the surface and cleaning the flow system from Cu(I) with 100 μL of 1 mM BC and 50 mM EDTA (injected at a flow rate of 5 μL/min).

The instrument was operated with separate eluent (1 × PBS, 0.005% surfactant P20, 1 μM EDTA, pH 7.4) and dispensor buffers (1 × PBS, 0.005% P20, 3 mM EDTA, pH 7.4) to give the instrument extra robustness with respect to possible contaminating metal ions that could interfere with ligand binding. SPR buffers and solutions were filtered and degassed before use.

For kinetic measurements, peptides were injected onto the surface by using the KINJECT command, and sensorgrams were analyzed using the BIAevaluation 3.0 program (BIACORE). The sensorgram was allowed to run for an additional 20 min after the end of injection to determine the dissociation kinetics. Kinetic constants were obtained by fitting curves to a single-site binding model (A + B = AB).

Q-TOF Mass Spectrometry. Peptides eluting from the Cu−NTA chip surface were collected and analyzed by Q-TOF-MS (API QSTAR Pulsar, PE Biosystems) in the positive

ion mode. The sample was desalted on a disposable C-18 reversed-phase column (ZipTip, Millipore, Bedford, MA), eluted with 70% methanol/1% acetic acid, and injected with a flow rate of 3 μL/min using the standard IonSpray source. Data were acquired using the standard instrument parameters and evaluated was performed with the PE SCIEX-Analyst software. Molecular mass of peptides was determined by using the measured monoisotopic *m*/*z* values. The instrument was calibrated according to the manufacturer's guidelines.

Inductively Coupled Plasma Mass Spectrometry (ICP-MS). For analysis of metal concentrations, the samples were diluted in 5% HNO_3 solution. ICP-MS was performed using a HP4500 Series 300 ShieldTorch System instrument (Agilent, Waldbronn, Germany) in peak-hopping mode with spacing at 0.05 amu, 3 points/peak, 5 scans/replicate, 2−3 replicates/sample, and an integration time of 400 ms/point. The rate of plasma flow was 15 L/min with an auxiliary flow of 1.0 L/min. The RF power was 1.2 kW. The sample was introduced using a cross-flow nebulizer at a flow rate of 1.06 L/min. The apparatus was calibrated using a 5% HNO_3 solution containing Cu at 5, 10, 25, 50, and 100 ppb with ^{103}Rh, the internal standard for all isotopes of Cu.

Circular Dichroism Spectroscopy. Alterations in the secondary structure content of the APP/APLP peptides was monitored by circular dichroism spectroscopy. Spectra were taken using a Jasco J-710 instrument with a PFD-350S temperature control device set at a sensitivity of 10 mdeg, a time constant of 4 s, and a scan speed of 5 nm/min. Typically, protein at 100 μg/mL in 1 mM Tris-HCl buffer (pH 7.5) plus either 100 μM Cu(II) or 100 μM EDTA was measured in a 1 mm quartz cuvette, scanning from 240 to 190 nm. Protein concentrations for the calculation of mean residue ellipticity (Θ_{mrw}) were determined by amino acid analysis of the sample after measurement. Curves are presented as the signal average of four transients with a similarly signal-averaged baseline subtracted. A Fourier transform operation was carried out to remove high-frequency noise from the signal.

Secondary structure content of the peptides was estimated from the far UV CD spectra as mean residue ellipticity using the PEPFIT program.

RESULTS

SPR Assay for Measuring Cu Binding. A biosensor assay based on surface plasmon resonance (SPR) analysis was established to measure the binding of CuBD peptides of APP, APP family paralogs (amyloid precursor-like proteins APLP1 and APLP2), and their orthologs (e.g., from *D. melanogaster*, *X. laevis*, *C. elegans*) to NTA-chelated Cu(II). The metal affinity chromatography matrix on the sensor chip, NTA, has four chelating sites that interact with four of the six coordination sites of divalent metal ions (Qiagen News (1996), Issue No. 5, Basel, Switzerland). Cu(II) has six coordination sites, and the favored stereochemistry of Cu(II) is an octahedral arrangement with six ligands (*31*). Therefore, the remaining two sites are free to interact with two amino acids, such as tyrosine, serine, threonine, or histidine (Figure 1A). Thus, the assay in the present report is based on the formation of an intermediate ternary complex of NTA−Cu(II)−peptide on the chip surface, which specifically allows for the analysis of Cu(II) binding on Cu(II)-loaded NTA−dextran affinity sensors.

To validate the working principle of our assay system, the following results are important to mention. First, no peptide binding was observed to the metal-free NTA surface (Figure 1A, red curve). Second, the pretreatment of the Cu(II)-charged NTA surface with the Cu(I)-specific chelator bathocuproine disulfonate (BC) (*32*) did not affect peptide binding (Figure 1B, black curve). This establishes that any peptide binding to Cu−NTA was specific and exclusively mediated by Cu(II). Third, when the Cu(II)-charged NTA surface was treated with tris(2-carboxyethyl)phosphine (TCEP) (Figure 1B, red curve) or vitamin C (Figure 1B, blue curve) alone, both agents effectively removed the metal from the surface by reducing Cu(II) to Cu(I) (Figure 1B). This demonstrates that the NTA−Cu(II) complex was abolished on the surface by TCEP or by vitamin C which both can reduce Cu(II) to Cu(I) and displace Cu(I) form NTA. TCEP is a nonsulfhydryl-based reductant which reduces oxidized thiol groups in proteins without forming adducts or noxious byproducts (*33*). TCEP is used in preference to the commonly used dithiothreitol (DTT) in our assay system to maintain peptides in their reduced state on the chip surface and to analyze Cu(II) binding to these peptides.

SPR Analysis of Copper-Binding Domains. To correlate the contrasting activities of APP_{CuBD} peptides from divers orthologs and paralogs (Table 1) (*28*), we determined the dissociation kinetics of these peptides (Figure 2A; Table 2). The results reveal that any conversion of Cu(II) to Cu(I) is a rate-limiting reaction of peptide−Cu complex formation and maintenance. A decreasing response signal (Figure 2A) is termed "displacement" because it starts at ∼950−970 s and, therefore, is prior to the real dissociation phase starting at ∼1070 s. This is observed when maximum binding capacity to Cu(II)−NTA is reached at ∼950 s (Figure 2A, panels A−H) and the injection of peptide solutions is continued to ∼1080 s. During this time interval, the peptides exhibit displacement activities of peptide−Cu(I) complexes due to their Cu(II)-reducing activities and the inability of NTA to bind Cu(I) (Figure 2A, black curves). Thus, each sensorgram monitors the stability of the ternary peptide−Cu(II)−NTA complex that governs the reaction rate. Because the dissociation of the complex is limited by the peptide, then the peptide affinity for Cu(II) (i.e., for Cu(II)−NTA) could be measured. Because of the rapid association (at ∼950 s; Figure 2A), we were unable to carry out a complete kinetic analysis of the association process (with a duration of less than 10 s). However, the sensorgrams in Figure 2A were evaluated for mean displacement and dissociation rate constants. The BIACORE data (Table 2) has been analyzed according to kinetic studies of mobilization of bound Cu(II) from human serum albumin with chelating agents involving an intermediate ternary complex with the rate constant k_1 as the speed-limiting determinant (*34*).

SPR Analysis of Copper-Binding Domains with BC. To correlate the dependence of APP_{CuBD} binding to Cu(II)-charged NTA with Cu(II) reduction activity, we injected individual peptides without any additives (Figure 2A, panels A−H, black curves) or in the presence of a ∼10-fold molar excess of BC (Figure 2A, panels A−H, blue curves). Under these conditions, BC successfully competed for Cu(I) binding with those peptides that are able to reduce Cu(II) to Cu(I) and to form peptide−Cu(I) complexes. When Cu(I) was generated from the Cu(II)−NTA complexes, the Cu(I)−

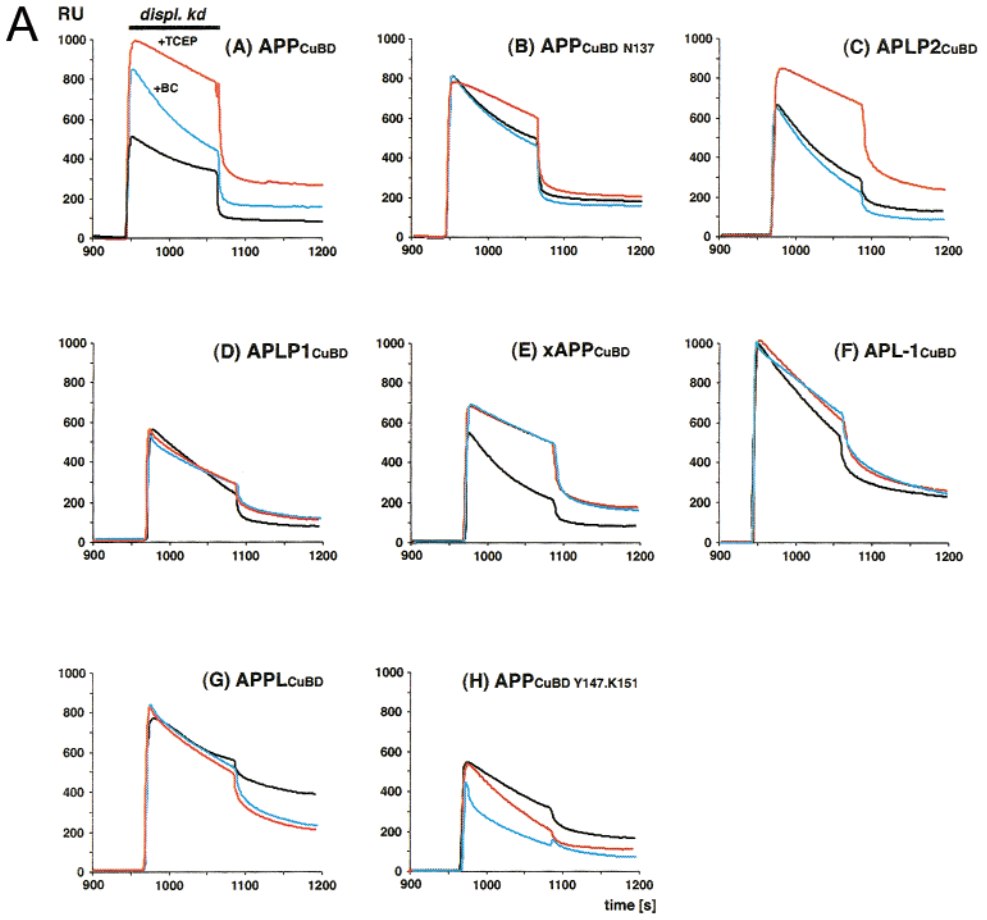

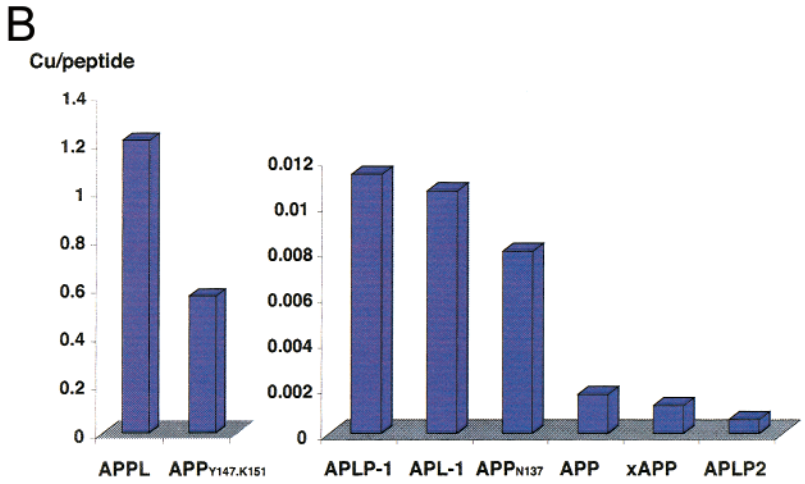

FIGURE 2: (A) Sensorgram showing the capturing of CuBDs by the Cu(II)-charged NTA surface. APP_{CuBD} (panel A), APP_{CuBD} N137 (panel B), $APLP2_{CuBD}$ (panel C), $APLP1_{CuBD}$ (panel D), $xAPP_{CuBD}$ (panel E), $APL\text{-}1_{CuBD}$ (panel F), $APPL_{CuBD}$ (panel G), and APP_{CuBD} Y147.K151 (panel H) were injected onto Cu(II)−NTA at a flow rate of 5 μL/min for 100 s, without any additives (series 1, black curve), in the presence of BC (series 2, blue curve) or in the presence of TCEP (series 3, red curve). After the injection with a very fast association, a rapid displacement is followed by a slower dissociation phase. Material eluting form the NTA surface was subjected to Q-TOF-MS analysis. Change in the baseline after the injection corresponds to the amount of peptide bound to the sensor surface of the flow cell. (B) Investigation of the lability of peptide−Cu complexes in aqueous systems under equilibrium conditions. Cu/peptide molar ratios of CuBDs are obtained by ICP-MS analysis after HPLC separation of peptide−Cu complexes (initial metal-to-ligand ratio: 200). APPL possesses lower rates of dissociation relative to the following ones (from left to right). The error in all reported values of at least two separate experiments is less than 6%.

peptide complexes were immediately displaced from the NTA surface, as indicated by decreasing response units during the injection phase (Figure 2A, panels A−H).

Because of the presence of BC, the Cu(II) binding capacity (at ~950 s) increased by 78% ± 5% for APP_{CuBD} and 22% ± 2% for $xAPP_{CuBD}$ (i.e., maximum response of black and blue curves in Figure 2A, panels A and E). However, the maximum response of the other peptides remained unaffected by BC. This indicates that BC successfully competed with the peptides APP_{CuBD} (panel A) and $xAPP_{CuBD}$ (panel E) for

Table 2: Kinetic Analysis of CuBD Binding to Cu(II)−NTA by SPR[a]

	control		BC		TCEP	
CuBDs	displ k_d $[s^{-1}] \times 10^{-3}$	diss k_d $[s^{-1}] \times 10^{-3}$	displ k_d $[s^{-1}] \times 10^{-3}$	diss k_d $[s^{-1}] \times 10^{-3}$	displ k_d $[s^{-1}] \times 10^{-3}$	diss k_d $[s^{-1}] \times 10^{-3}$
APP	4.4	1.6	6.4	1.1	2.4	1.9
APP_{N137}	4.9	1.4	5.5	1.2	2.7	1.3
APLP2	8.2	2.5	10.1	2.8	2.4	3.4
APLP1	7.6	3.8	5.4	3.9	6.3	4.0
xAPP	9.4	1.9	3.0	1.8	3.2	2.7
APL-1	5.7	2.9	3.8	4.6	4.9	3.1
APPL	4.0	1.5	4.1	3.4	4.6	3.3
$APP_{Y147.K151}$	5.2	2.1	8.9	2.2	9.9	4.1

[a] displ, displacement; diss, dissociation.

Cu(I) during the injection phase (∼950 to ∼1100 s). Thus, peptides APP_{CuBD} and $xAPP_{CuBD}$ in their oxidized form (as analyzed and described in Figure 3) regained affinity for residual Cu(II)−NTA when they were already stripped of Cu(I) by BC during the injection.

The displacement rate of the peptide−Cu(I) complexes was decreased in the presence of BC during the injection phase for $APL\text{-}1_{CuBD}$ (1.5-fold; Figure 2A, panel F) and $xAPP_{CuBD}$ (3.1-fold; Figure 2A, panel E) but was accelerated 1.7-fold for the chimeric APP/APL-1 mutant peptide APP_{CuBD} Y147.K151 (Figure 2A, panel H). In contrast, no significant influence of BC was found on peptides APP_{CuBD} N137 (panel B), $APLP2_{CuBD}$ (panel C), $APLP1_{CuBD}$ (panel D), and $APPL_{CuBD}$ (panel G) (Figure 2A).

SPR Analysis of Copper-Binding Domains with TCEP. To investigate peptide binding to Cu(II)−NTA under conditions where the formation of a new disulfide bridge (between cysteines 144 and 158 around copper-binding histidine residues of APP) was inhibited (*13*), injections were performed in the presence of a 200-fold molar excess of TCEP. The interaction of the CuBD peptides with the Cu(II)−NTA biosensor surface under reducing conditions is shown in Figure 2A (red curves). Compared with the injection without any additives (Figure 2A, black curves), the presence of TCEP (Figure 2A, red curves) causes the maximum response to increase by 94% ± 5% for APP_{CuBD} (Figure 2A, panel A), 27% ± 2% for $APLP2_{CuBD}$ (Figure 2A, panel C), and 22% ± 2% for $xAPP_{CuBD}$ (Figure 2A, panel E). APP_{CuBD} exhibited an even higher maximum response (15% ± 2%) as compared to the injection in the presence of BC (Figure 2A, panel A, blue curve) and thus revealed the highest affinity for Cu(II) of all peptides under reducing conditions (see also Table 2).

In the presence of TCEP, the kinetic analysis shows strikingly slower displacement rates (>1.5-fold) for those peptides with a higher maximum binding rate (1.8-fold slower displacement rates for APP_{CuBD}, 3.4-fold for $APLP2_{CuBD}$, and 3.0-fold for $xAPP_{CuBD}$; Figure 2A, panels A, C, and E; Table 2). Interestingly and unlike all of the other peptides, a slower displacement rate was also observed for the mutant APP_{CuBD} N137 (1.8-fold) as the only striking difference (Figure 2A, panel B; Table 2). Thus, oxidation of APP_{CuBD} N137 was not inhibited although TCEP was present.

In the presence of TCEP, the displacement rates of $APL\text{-}1_{CuBD}$ and $APPL_{CuBD}$ were not significantly changed. In contrast, the mutant APP_{CuBD} Y147.K151 was found significantly increased (1.9-fold; Table 2; Figure 2A). In this case, TCEP stripped off Cu(II) from the NTA (by reducing Cu(II) to Cu(I) as observed in the control, Figure 1B) rather than being required to keep APP_{CuBD} Y147.K151 in its reduced state. This is due to the fact that CuBDs have an affinity to the NTA−Cu(II) surface and thus are shielding Cu(II) (bound to the NTA-surface) from the reducing agent TCEP which does not have an affinity to the chip surface at all and is uniformly distributed within the continuous buffer flow through the cartridge.

Taken together, those peptides possessing a conserved central histidine region (APP_{CuBD}, $APLP2_{CuBD}$, $xAPP_{CuBD}$, APP_{CuBD} N137; Figure 2A; Table 1) showed an increased binding to the Cu(II)-charged NTA surface in the presence of TCEP (APP_{CuBD}, $APLP2_{CuBD}$, $xAPP_{CuBD}$; Figure 2A, panels A−H) or much slower displacement rates (e.g., for APP_{CuBD}, $APLP2_{CuBD}$, $xAPP_{CuBD}$, and APP_{CuBD} N137; Figure 2A). On the basis of the dissociation rate constants measured (and disregarding the association rate constants which are too fast to be measured), the His-X-His motif peptides (Table 1) have a higher affinity for Cu(II)−NTA in their reduced states.

ICP-MS Analysis of CuBD−Copper Complexes. Residual Cu(II)/Cu(I)-binding activities of CuBDs after long-term incubation (HPLC purification of CuBD−copper complexes) were measured in solution by ICP-MS analysis. This was used as a complementing method to SPR analysis. Whereas the special stereochemistry of NTA−Cu(II) leaves the possibility open that there were only axial sites for binding the peptide (see Figure 1A), the effects of Cu(II)-reducing activities of CuBDs analyzed by SPR remained unconsidered by ICP-MS analysis.

Interestingly, the CuBDs of *Drosophila* APPL and the mutant $APP_{Y147.K151}$ exhibited exceptionally slow dissociation rates by ICP-MS (Figure 2B) and by SPR analysis (Figure 2A, panels G and H). Most likely, these two species formed kinetically stable peptide−Cu(II) complexes in solution in their oxidized but not in the reduced states, as is evident from the faster dissociation in the presence of TCEP (Figure 2A). The ranking for an accelerated dissociation among the peptide−Cu(II)/Cu(I) complexes in solution (Figure 2B) is APLP-1 (having a low binding capacity for NTA−Cu(II); SPR data in Figure 2A, panel D) and APL-1 (having a high binding capacity for NTA−Cu(II); SPR data in Figure 2A, panel F). Together with the SPR results (Figure 2A, panels D and F), the ICP-MS data indicates that both peptides have residual binding capacity for Cu(II) in their oxidized and in their reduced states. Those peptides that showed an increase in NTA−Cu(II) binding in their reduced states by SPR

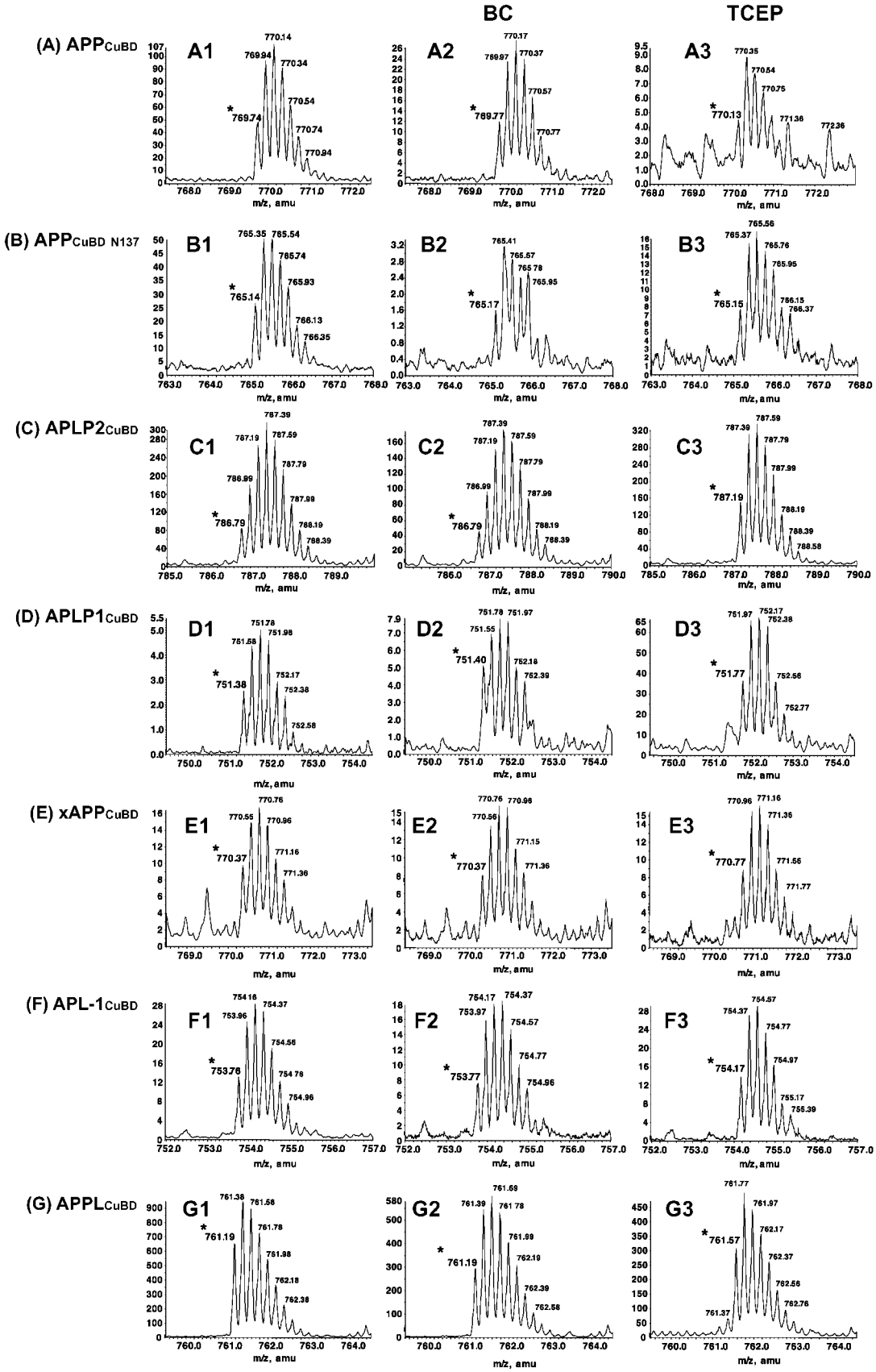

FIGURE 3: ESI-Q-TOF analysis of 5-times charged monoisotopic ions (star-labeled *m*/*z* values correspond to a peptide containing exclusively ^{12}C atoms) of peptide samples eluted and recovered from the NTA−chip surface: APP_{CuBD} (panel A), APP_{CuBD} N137 (panel B), $APLP2_{CuBD}$ (panel C), $APLP1_{CuBD}$ (panel D), $xAPP_{CuBD}$ (panel E), APL-1_{CuBD} (panel F), and $APPL_{CuBD}$ (panel G); series 1 without any additives, series 2 with BC, and series 3 with TCEP. Note that all CuBDs were found to be oxidized without any additives during the injection and in the presence of BC. All peptides except APP_{CuBD} N137 were found to be reduced by TCEP. Compare the star-labeled 5-times charged peptide ions, which differ by 0.4 atomic mass units between oxidized and reduced peptides. This difference represents a molecular weight shift of 2 Da due to the loss of two hydrogen atoms when the disulfide is formed.

(Figure 2A) displayed low levels of residual Cu(I) binding as indicated by ICP-MS (Figure 2B). These data suggest that slow dissociation of peptide−Cu complexes (APPL, $APP_{Y147.K151}$, APLP-1, and APL-1; Figure 2B) in combination with high capacity binding (APPL, $APP_{Y147.K151}$, and APL-1; Figure 2A) correlates with the protective activities measured in our cell culture and lipid peroxidation assays (*28*). Taken together, protective activities are largely characterized by avid Cu(II) binding of oxidized peptides and slow Cu(II) reduction.

Q-TOF Analysis of Peptides Eluted from Cu(II)−NTA Sensor Chip Surfaces. To investigate whether peptide binding to Cu(II)−NTA led to oxidative modification of the CuBD variants of APP via formation of an intramolecular cystine (*35*), the presence or absence of the disulfide was analyzed by Q-TOF-MS. Peptide samples were eluted from the NTA−chip surface and concentrated and desalted before analysis. Because of the high resolution of the ESI-Q-TOF-MS, the charge state of the ions could be determined from the mass spectrum (Figure 3). This allowed for the unambiguous determination of the monoisotopic molecular weight of the peptides. ESI-Q-TOF analysis is shown in Figure 3 for the 5-times charged monoisotopic ions (the star-labeled *m*/*z* peak corresponds to a peptide containing exclusively ^{12}C atoms).

To determine the reliability of this approach, peptides were dissolved in the same buffer used for the BIACORE experiments, desalted, concentrated, and analyzed by Q-TOF mass spectrometry before injection onto the NTA−sensor chip. This control experiment revealed that all of the individual CuBD peptides were present in their reduced state before the injection onto the Cu(II)−NTA surface (data not shown) and that Q-TOF mass spectrometry provides a fast approach to detect intramolecular disulfide bonds. Subsequently, MS measurements of the peptides recovered from the Cu(II)-charged NTA sensor chip surface revealed *m*/*z* values for the 5-times charged peptide ions which differ by 0.4 atomic mass units between oxidized and reduced peptides. This difference represents a molecular weight shift of 2 Da due to the loss of two hydrogen atoms when the disulfide bond is formed. Thus, the cysteine residues of CuBD peptides (with identical cysteine spacings; Table 1) had spontaneously generated a disulfide bond under the oxidizing conditions, both in the absence of BC (Figure 3, panels A−G, series 1) and in the presence of BC (Figure 3, panels A−G, series 2). These data show that (i) an intrachain disulfide linkage was formed exclusively and homogeneously in all peptides, (ii) an intermolecular disulfide-linked dimerization did not occur, and (iii) the formation of the intrachain disulfide linkage was not influenced by BC. Because the RECOVER (i.e., collecting the sample during the injection phase) and not the FRACTIONATE BIACORE command was used to collect the eluting peptide from the NTA−sensor surface, we can conclude that all peptides already contained the disulfide bond during the displacement phase (Figure 2A) and kinetic analyses of the displacement and dissociation phases are valid for oxidized peptides (except those done in the presence of TCEP) (Figure 2A; Table 2).

MS measurements of peptides in the presence of TCEP (Figure 3, panels A−G, series 3) confirmed that peptides APP_{CuBD}, $APLP2_{CuBD}$, $APLP1_{CuBD}$, $xAPP_{CuBD}$, $APL\text{-}1_{CuBD}$, and $APPL_{CuBD}$ were analyzed by SPR in the reduced forms. Obviously, the peptide APP_{CuBD} N137 (Figure 3B) was quickly oxidized by atmospheric oxygen after BIACORE analysis (Figure 2A) and before Q-TOF-MS analysis. This is further supported by the observation that this peptide was observed mainly in its oxidized state by Q-TOF-MS, even when the peptide was injected onto the Cu(II)−NTA−sensor chip surface with a ∼200-fold molar excess of TCEP (Figure 3, panel B3).

Thus, we conclude that CuBD peptides APP_{CuBD}, $APLP2_{CuBD}$, $xAPP_{CuBD}$, and APP_{CuBD} N137 can be classified into a group of peptides having an increased maximum binding to Cu(II)−NTA in its reduced form and a significantly slower displacement rate of peptide−Cu(I) complexes (Figure 2A, panels A−C and E). These data suggest a link between the inherent chemical properties of the peptides (i.e., the formation of an intramolecular disulfide bond) and the copper-mediated lipoprotein oxidation and neurotoxicity potential observed for the same group of APP_{CuBD} peptides in our neuronal toxicity culture assay (*28*).

In contrast, the maximum response of a second group of peptides (Figure 2A; Table 1) remained unchanged by TCEP. This indicates that these peptides bind equally well to the Cu(II)−NTA surface, irrespective of their oxidation state. In addition, they showed Cu(II)-reducing activities as is evident from the release of Cu(I)−peptide complexes from the chip surface (Figure 2A; panels F−H). The presence of BC did not cause a change, indicating that this second group of peptides can bind Cu(II) or Cu(I) equally well (Figure 2A).

Thus, this type of accuracy provided by SPR and mass spectrometry offered useful tools for an elucidation of the mechanism for the toxicity (*15*, *35*, *36*) of residues 142−166 of APP that can be attributed to Cu(II) reduction and Cu(II)/Cu(I) binding affinity indirectly measured by SPR analysis.

Circular Dichroism Spectroscopy. Because the displacement of Cu(I) complexes from the chip surface was due to a distinct stereochemistry of Cu(I) that favors a tetrahedral conformation and interferes with the coordination by NTA (Qiagen News (1996), Issue No. 5, Basel, Switzerland), we used CD spectroscopy to investigate the influence of Cu binding on conformational changes of peptides in solution. The far UV CD spectra were obtained for the various CuBD peptides, either complexed with copper (Figure 4, panels A−H, continuous line in B−H) or in its absence and in the presence of a chelator (i.e., EDTA) (Figure 4, panels B−H, broken line).

A selective and time-dependent degradation of APP_{CuBD} was observed upon the exposure of the peptide to Cu(II) in solution (Figure 4A). A mass spectrometric analysis revealed that the peptide was N- and C-terminally truncated (Multhaup, G., and Ruppert, T., unpublished observation), most likely due to the residual presence of reactive oxygen species in the buffer. This indicates that the APP_{CuBD} catalyzed a free radical-mediated secondary reaction driven by the rapidly formed Cu(I), as we have described for recombinant full-length APP (*35*).

Even without detailed secondary structure analysis, it is apparent that the absence of copper causes a significant alteration in the spectra of the group of peptides that preferentially bind Cu(II) in their reduced states (Figure 2A). All of them show a marked increase in the negative maximum at ∼198 nm, indicative of a less-ordered structure

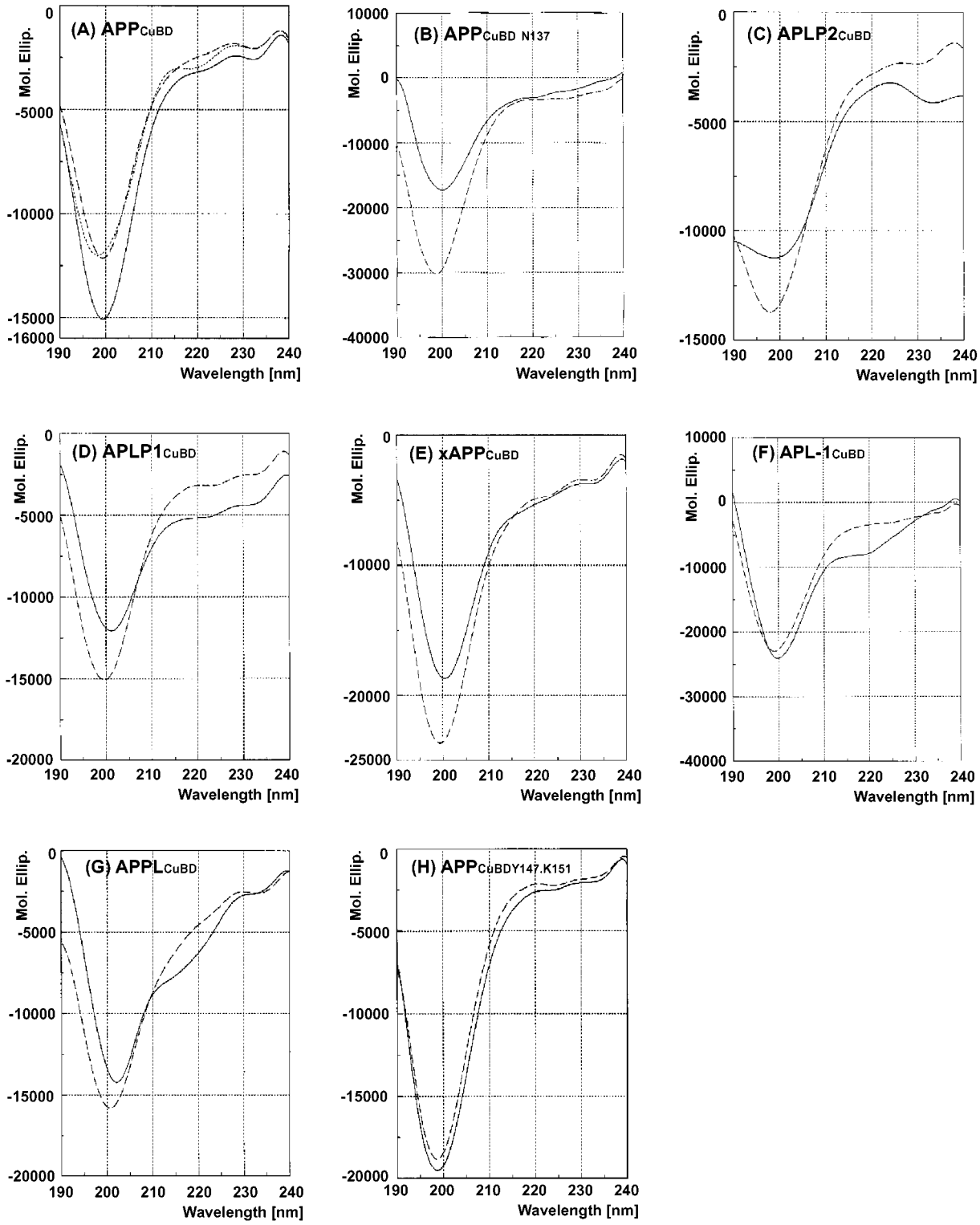

FIGURE 4: CD spectra of CuBDs were recorded at room temperature and in aqueous solutions immediately after preparing the solutions. The CD spectra of the APP_{CuBD} showed a time-dependent change (panel A). The shape of the APP_{CuBD} spectra (panel A) suggested that this peptide has lost secondary structure in the presence of 100 μM Cu(II) after 10 min incubation in the spectrometer without any further change thereafter (solid line represents measurement at time 0, dashed line after 10 min, dotted line after 24 h). Spectra of APP_{CuBD} N137 (panel B), $APLP2_{CuBD}$ (panel C), $APLP1_{CuBD}$ (panel D), $xAPP_{CuBD}$ (panel E), APL-1_{CuBD} (panel F), $APPL_{CuBD}$ (panel G), and APP_{CuBD} Y147.K151 (panel H) were recorded in the presence of 100 μM Cu(II) shown as a solid line and as a dashed line for 1 mM EDTA. Note that the β-sheet folding of APL-1 (C) rises with EDTA, whereas the foldings of orthologs either remain constant or become disordered in the absence of Cu(II).

(Figure 4, panels A−C and E). In contrast, the second group of peptides binds Cu(II) and Cu(I) equally well, independent of their oxidation state (Figures 2A,B and 3). They either show no change at this wavelength (Figure 4, panels F−H) or only relatively minor changes occur between the Cu-bound and nonbound states. Examination of alterations in intensity reveals that the conformational change occurring in the peptides APP_{CuBD} (Figure 4, panel A; data not shown for

EDTA), APP_{CuBD} N137 (panel B), $APLP2_{CuBD}$ (panel C), and $xAPP_{CuBD}$ (panel E) is principally due to a loss of ordered structure in the absence of copper. In contrast, APL-1_{CuBD} (panel F), $APPL_{CuBD}$ (panel G), and APP_{CuBD} Y147.K151 (panel H) tend to exhibit little changes. Moreover, the *C. elegans* peptide APL-1_{CuBD} (panel F) becomes more structured when copper is removed. Finally, the $APLP1_{CuBD}$ peptide (panel D), which yields ambiguous results in the SPR (Figure 2), exhibits an intermediate level of change.

DISCUSSION

The present study utilizes ESI-Q-TOF, ICP-MS, and CD spectroscopy to examine directly the role of APP family members in copper binding and reduction. Although APP is known to impair the copper balance in vivo ($APP^{0/0}$ mice have significantly elevated Cu levels in the liver and in the cerebral cortex), the role of other APP family members in copper binding has not been determined yet (*19*). Therefore, sophisticated techniques were applied to study the metal−peptide exchange reactions of the CuBDs of APP family members.

The data presented herein revealed a previously unappreciated complexity of APP family members, irrespective of binding and release of this metal ion. (i) Unexpectedly, APP homologues with and without conserved histidine residues at positions 147 and 151 all bind Cu(II). (ii) The kinetics of these reactions revealed an initial reduction of Cu(II) and a rapid displacement of Cu(I) complexes from the NTA surface in a metal redistribution process between Cu(II)−NTA and the variant CuBDs. (iii) Oxidized peptides were the kinetically favored products within this redox reaction, resulting in a new disulfide bond in all peptides. (iv) This reaction was fastest for human APP_{CuBD} and depended on the individual chelating residues (see Table 1).

After testing a variety of chromatographic conditions, the NTA−sensor chip surface provided a rapid and effective means of monitoring Cu(II) binding and reduction in the absence or the presence of BC or TCEP to alter specifically the state of peptide−Cu interactions.

Peptide−Cu(II)−NTA complexes are only stable when the peptide ligands surround the central ion in its favored geometry. Cu(I)−ligands favor a tetrahedral conformation, while Cu(II) favors a square planar conformation when steric hindrance is excluded (*31*). In the case of Cu(II)−NTA, the reduction of Cu(II) to Cu(I) interferes with Cu(II) binding to NTA due to the inability to provide a tetrahedral arrangement that is preferred by Cu(I). Therefore, a rapid displacement of Cu(I)−peptide complexes from the NTA surface was observed for APP_{CuBD}, $APP_{CuBD\ N137}$, $APLP2_{CuBD}$, and $xAPP_{CuBD}$ and further confirmed by ICP-MS and Q-TOF-MS. APP_{CuBD}, APP_{CuBD} N137, $APLP2_{CuBD}$, and $xAPP_{CuBD}$ (Table 1) all contain the central histidine region at positions 147, 149, and 151. Histidine residues are common ligands for Cu(I) sites (*31*); thus, the specific stereochemistry of Cu(I) coordination most likely determines the strong redox potential of APP_{CuBD}, APP_{CuBD} N137, $APLP2_{CuBD}$, and $xAPP_{CuBD}$ observed by SPR analysis. This is similar to redox-active centers of proteins or enzymes where conversion between the oxidation states Cu(I) and Cu(II) can be achieved when copper is coordinated in part by ligands favoring Cu(I) and in part by others favoring Cu(II) (*37*). The redox activity of APP and its homologues may be critical to the ability to transport copper, supported by the finding that Cu reduction is somehow linked with copper uptake in eukaryotic cells (*38*).

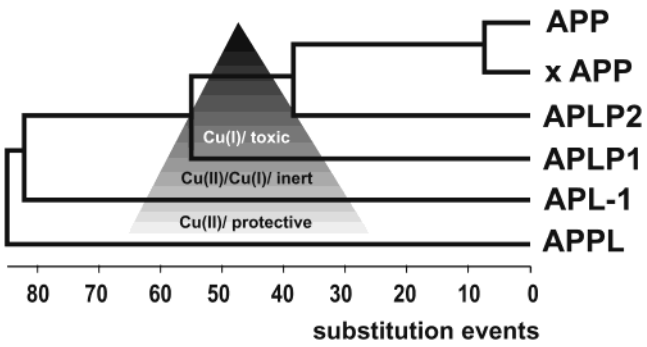

FIGURE 5: Evolution of APP gene family as aligned sequences (MEGALIGN-Phylogeny, Lasergene System by DNASTAR Inc.) in a phylogenetic tree to determine the ancestral relationships between CuBDs; APP, Homosapiens amyloid precursor protein; xAPP, *Xenopus laevis* amyloid-like protein precursor; APLP1, Homosapiens amyloid-like protein 1 precursor; APLP2, Homosapiens amyloid-like protein 2 precursor; APL-1, *Caenorhabditis elegans* amyloid-like protein precursor; APPL, *Drosophila melanogaster* amyloid-like protein precursor. The length of each pair of branches represents the distance between sequence pairs. The scale beneath the tree measures the distance between sequences. Units indicate the number of substitution events. Invertebrate APL-1 and APPL form a fourth functional lineage that is ancestral to the other vertebrate APPs.

A much slower protein−metal exchange reaction was observed for APLP1, the most ancestral form of the APP family (*39*). The APLP1 peptide, which had an inert phenotype in the toxicity assay (*28*) was poorly influenced by copper due to the lack of clustered histidine residues His147 and His149 in its center (Table 1). Here, Cu(II) may be coordinated by the amino acids serine, threonine, or histidine outside of the amino acids which are enclosed by two cysteines (homologous to APP residues Cys144 and Cys158). In APLP1 complexes, Cu(I) may also be complexed by Met141 which is conserved from APLP1 to higher homologues (Table 1).

The key observation, which leads to the conclusion that copper binding developed to Cu(II) reducing activities of APP family members along the eukaryotic evolutionary line (Figure 5) is that APPL and APL-1 can achieve very stable binding configurations to Cu(II) and to Cu(I), as shown by SPR analysis and concluded from ICP-MS and Q-TOF-MS data. This can only be achieved when copper is coordinated in part by ligands favoring Cu(I) and in part by others favoring Cu(II). In APL-1, Cu(II) may be coordinated by the amino acids tyrosine and histidine inside and serine and threonine outside of the conserved cysteine residues (Table 1). In APPL, only histidine residues outside of the APP conserved residues may be responsible of Cu(II) binding (Table 1). Thus, APPL and APL-1 resemble electron transport proteins which function by switching from Cu(II) to Cu(I) coordination with stereochemistries that lay between both preferred oxidation states. Drosophila flies deleted of the Appl gene are viable, fertile, and morphologically normal, but they nevertheless exhibit subtle behavioral deficits (*40*). In contrast, the *C. elegans* APL-1 molecule has an essential function. When sequences containing the CuBD of the apl-1 gene are removed, the homozygous knockout worms show

a larval phenotype representing a complete loss of function (*41*). APL-1 could be truly essential for Cu transport or protein sequestration of Cu(II) ions (*42*−*44*). Our data suggest that APL-1 and APPL can shift the Cu(II)-binding equilibrium from the exchangeable Cu(II) pool to the tightly bound nonexchangeable pool and, thus, prevent ROS formation.

APL-1 was predicted to be the closest to the ancestral proteins (Figure 5), which shares many similarities with the human APP (*45*). However, important functions of specific APP domains will be different from the paralogs APLP1, APLP2, APPL, and APL-1. In APP and higher evolved APP homologues, there is a gain in activity toward promoting Cu(II) reduction. In so far, APP as a type-I transmembrane protein resembles a membrane anchored Cu(II)-reductase although there is no evidence of a catalytic activity. Alternatively, APP may act in its secreted form as a Cu(I) transport protein.

In any case, differing metal binding of APP may contribute to the etiology of Alzheimer's disease, such as aberrant metal binding by prion protein in human prion disease (*10*). Because of an impairment of copper balance which predisposes neuronal cells to apoptosis by oxidative stress (*46*), an altered metal ion occupancy of APP and its paralogs APLP1 and APLP2 may play a pivotal role in the pathogenesis of AD.

ACKNOWLEDGMENT

We thank Gabi Becker and Helmut E. Meyer, Ruhr-Universität Bochum, Institut für Physiologische Chemie I, for help with the amino acid analysis and John Williams for critical reading the manuscript.

REFERENCES

1. Atwood, C. S., Huang, X., Moir, R. D., Tanzi, R. E., and Bush, A. I. (1999) *Met. Ions Biol. Syst. 36*, 309−364.
2. Smith, M. A., and Perry, G. (1995) *J. Neurol. Sci. 134 Suppl*, 92−94.
3. Multhaup, G., and Masters, C. L. (1999) *Met. Ions Biol. Syst. 36*, 365−387.
4. Milhavet, O., McMahon, H. E., Rachidi, W., Nishida, N., Katamine, S., Mange, A., Arlotto, M., Casanova, D., Riondel, J., Favier, A., and Lehmann, S. (2000) *Proc. Natl. Acad. Sci. U.S.A. 97*, 13937−13942.
5. Yim, M. B., Chock, P. B., and Stadtman, E. R. (1990) *Proc. Natl. Acad. Sci. U.S.A. 87*, 5006−5010.
6. Brown, D. R. (2001) *Brain Res. Bull. 55*, 165−173.
7. Bush, A. I. (2000) *Curr. Opin. Chem. Biol. 4*, 184−191.
8. Waggoner, D. J., Bartnikas, T. B., and Gitlin, J. D. (1999) *Neurobiol. Dis. 6*, 221−230.
9. Strausak, D., Mercer, J. F., Dieter, H. H., Stremmel, W., and Multhaup, G. (2001) *Brain Res. Bull. 55*, 175−185.
10. Wong, B. S., Brown, D. R., Pan, T., Whiteman, M., Liu, T., Bu, X., Li, R., Gambetti, P., Olesik, J., Rubenstein, R., and Sy, M. S. (2001) *J. Neurochem. 79*, 689−698.
11. Liu, H., Zhu, H., Eggers, D. K., Nersissian, A. M., Faull, K. F., Goto, J. J., Ai, J., Sanders-Loehr, J., Gralla, E. B., and Valentine, J. S. (2000) *Biochemistry 39*, 8125−8132.
12. Corson, L. B., Strain, J. J., Culotta, V. C., and Cleveland, D. W. (1998) *Proc. Natl. Acad. Sci. U.S.A. 95*, 6361−6366.
13. Multhaup, G., Schlicksupp, A., Hesse, L., Beher, D., Ruppert, T., Masters, C. L., and Beyreuther, K. (1996) *Science 271*, 1406−1409.
14. Scheuermann, S., Hambsch, B., Hesse, L., Stumm, J., Schmidt, C., Beher, D., Bayer, T. A., Beyreuther, K., and Multhaup, G. (2001) *J. Biol. Chem. 276*, 33923−33929.
15. Hesse, L., Beher, D., Masters, C. L., and Multhaup, G. (1994) *FEBS Lett. 349*, 109−116.
16. Borchardt, T., Camakaris, J., Cappai, R., Masters, C. L., Beyreuther, K., and Multhaup, G. (1999) *Biochem. J. 344*, 461−467.
17. Lau, K. F., McLoughlin, D. M., Standen, C., and Miller, C. C. (2000) *Mol. Cell Neurosci. 16*, 557−565.
18. McLoughlin, D. M., Standen, C. L., Lau, K. F., Ackerley, S., Bartnikas, T. P., Gitlin, J. D., and Miller, C. C. (2001) *J. Biol. Chem. 276*, 9303−9307.
19. White, A. R., Reyes, R., Mercer, J. F., Camakaris, J., Zheng, H., Bush, A. I., Multhaup, G., Beyreuther, K., Masters, C. L., and Cappai, R. (1999) *Brain Res. 842*, 439−444.
20. Roelofsen, H., Wolters, H., Van Luyn, M. J., Miura, N., Kuipers, F., and Vonk, R. J. (2000) *Gastroenterology 119*, 782−793.
21. O'Halloran, T. V., and Culotta, V. C. (2000) *J. Biol. Chem. 275*, 25057−25060.
22. Martins, R. N., Harper, C. G., Stokes, G. B., and Masters, C. L. (1986) *J. Neurochem. 46*, 1042−1045.
23. Smith, M. A., Harris, P. L., Sayre, L. M., and Perry, G. (1997) *Proc. Natl. Acad. Sci. U.S.A. 94*, 9866−9868.
24. Sayre, L. M., Perry, G., Atwood, C. S., and Smith, M. A. (2000) *Cell Mol. Biol. 46*, 731−741.
25. Atwood, C. S., Moir, R. D., Huang, X., Scarpa, R. C., Bacarra, N. M., Romano, D. M., Hartshorn, M. A., Tanzi, R. E., and Bush, A. I. (1998) *J. Biol. Chem. 273*, 12817−12826.
26. Cherny, R. A., Legg, J. T., McLean, C. A., Fairlie, D. P., Huang, X., Atwood, C. S., Beyreuther, K., Tanzi, R. E., Masters, C. L., and Bush, A. I. (1999) *J. Biol. Chem. 274*, 23223−23228.
27. Huang, X., Atwood, C. S., Hartshorn, M. A., Multhaup, G., Goldstein, L. E., Scarpa, R. C., Cuajungco, M. P., Gray, D. N., Lim, J., Moir, R. D., Tanzi, R. E., and Bush, A. I. (1999) *Biochemistry 38*, 7609−7616.
28. White, A. R., Multhaup, G., Galatis, D., McKinstry, W. J., Parker, M. W., Pipkorn, R., Beyreuther, K., Masters, C. L., and Cappai, R. (2002) *J. Neurosci. 22*, 365−376.
29. Merrifield, R. B. (1963) *J. Am. Chem. Soc. 85*, 2149.
30. Carpino, L. A., and Han, G. Y. (1972) *J. Org. Chem. 37*, 3404−3409.
31. Abolmaali, B., Taylor, H. V., and Weser, U. (1998) in *Structure & Bonding; Bioinorganic chemistry; Trace element evolution from anaerobes to aerobes* (Williams, R. J. P., Ed.), pp 91−190, John Wiley, Berlin, Germany.
32. Huang, X., Cuajungco, M. P., Atwood, C. S., Hartshorn, M. A., Tyndall, J. D., Hanson, G. R., Stokes, K. C., Leopold, M., Multhaup, G., Goldstein, L. E., Scarpa, R. C., Saunders, A. J., Lim, J., Moir, R. D., Glabe, C., Bowden, E. F., Masters, C. L., Fairlie, D. P., Tanzi, R. E., and Bush, A. I. (1999) *J. Biol. Chem. 274*, 37111−37116.
33. Gray, W. R. (1993) *Protein Sci. 2*, 1732−1748.
34. Gao, L. M., Li, R. C., Wang, K., Getz, E. B., Xiao, M., Chakrabarty, T., Cooke, R., and Selvin, P. R. (1989) *J. Inorg. Biochem. 36*, 83−92.
35. Multhaup, G., Ruppert, T., Schlicksupp, A., Hesse, L., Bill, E., Pipkorn, R., Masters, C. L., and Beyreuther, K. (1998) *Biochemistry 37*, 7224−7230.
36. White, A. R., Multhaup, G., Maher, F., Bellingham, S., Camakaris, J., Zheng, H., Bush, A. I., Beyreuther, K., Masters, C. L., and Cappai, R. (1999) *J. Neurosci. 19*, 9170−9179.
37. Murphy, L. M., Strange, R. W., and Hasnain, S. S. (1997) *Structure 5*, 371−379.
38. Hassett, R., and Kosman, D. J. (1995) *J. Biol. Chem. 270*, 128−134.
39. Coulson, E. J., Paliga, K., Beyreuther, K., and Masters, C. L. (2000) *Neurochem. Int. 36*, 175−184.
40. Luo, L., Tully, T., and White, K. (1992) *Neuron 9*, 595−605.
41. Hornsten, A., Hausmann, R. E., and Li, C. (1999) SFN Conference Abstract 818.13.
42. Multhaup, G., Strausak, D., Bissig, K. D., and Solioz, M. (2001) *Biochem. Biophys. Res. Commun. 288*, 172−177.
43. Solioz, M., Odermatt, A., and Krapf, R. (1994) *FEBS Lett. 346*, 44−47.
44. Huffman, D. L., and O'Halloran, T. V. (2001) *Annu. Rev. Biochem. 70*, 677−701.
45. Daigle, I., and Li, C. (1993) *Proc. Natl. Acad. Sci. U.S.A. 90*, 12045−12049.
46. Rossi, L., Marchese, E., Lombardo, M. F., Rotilio, G., and Ciriolo, M. R. (2001) *Free Radical Biol. Med. 30*, 1177−1187.
47. Tainer, J. A., Getzoff, E. D., Richardson, J. S., and Richardson, D. C. (1983) *Nature 306*, 284−287.

BI0258647